



ARTICLE

<https://doi.org/10.1038/s41467-019-11130-y>

OPEN

Strong coupling of collective intermolecular vibrations in organic materials at terahertz frequencies

Ran Damari^{1,2}, Omri Weinberg^{1,2}, Daniel Krotkov¹, Natalia Demina¹, Katherine Akulov¹, Adina Golombek¹, Tal Schwartz ^{1,3} & Sharly Fleischer ^{1,3}

Several years ago, strong coupling between electronic molecular transitions and photonic structures was shown to modify the electronic landscape of the molecules and affect their chemical behavior. Since then, this concept has evolved into a new field known as polaritonic chemistry. An important ingredient in the progress of this field was the demonstration of strong coupling with intra-molecular vibrations, which enabled the modification of processes occurring at the electronic ground-state. Here we demonstrate strong coupling with collective, inter-molecular vibrations occurring in organic materials in the low-terahertz region ($\lesssim 10^{12}$ Hz). Using a cavity filled with α -lactose molecules, we measure the temporal evolution and observe coherent Rabi oscillations, corresponding to a splitting of 68 GHz. These results take strong coupling into a new class of materials and processes, including skeletal polymer motions, protein dynamics, metal organic frameworks and other materials, in which collective, spatially extended degrees of freedom participate in the dynamics.

¹School of Chemistry, Raymond and Beverly Sackler Faculty of Exact Sciences and Tel Aviv University Center for Light-Matter Interaction, Tel Aviv University, Tel Aviv 6997801, Israel. ²These authors contributed equally: Ran Damari, Omri Weinberg. ³These authors jointly supervised: Tal Schwartz, Sharly Fleischer. Correspondence and requests for materials should be addressed to T.S. (email: talschwartz@tau.ac.il) or to S.F. (email: sharlyf@tauex.tau.ac.il)

In the strong coupling regime, the interaction between light and matter overcomes all the incoherent and dissipative processes, which profoundly changes its nature. In this regime, the wavefunctions of the photons and the material excitations are coherently mixed to form hybrid light-matter quantum states known as polaritons¹. This fascinating phenomenon has been observed in many different types of material systems, such as cold atoms^{2–4}, excitons in semiconductors^{5,6}, electronic spins in nitrogen-vacancy centers⁷, phonons in inorganic crystals^{8–11}, and many others. Among these, strong coupling with organic molecules^{12,13} has seen an ever-increasing interest in recent years, both in conventional Fabry–Pérot cavity systems as well as in plasmonic structures¹⁴. Interestingly, the creation of the polaritonic wavefunctions under strong coupling and the modification of the energetic landscape of the molecules can have a significant influence on the physical and chemical properties of the molecules^{1,15,16}, affecting the rates and yields of chemical reactions^{17–22}, their emission properties^{23–25}, electronic and excitonic transport^{26–30} and more. This new field, known as polaritonic chemistry, is currently under intense study, both experimentally and theoretically. While traditionally, strongly coupled organic systems involved the coupling of an optical resonance to electronic transitions in molecules (Frenkel excitons), recently, vibrational strong coupling has been introduced as a new paradigm^{31–36}. In such systems, a particular intramolecular, optically active vibrational transition is coupled to a mid-infrared resonator, creating hybrid excitations termed “vibro-polaritons”. As has been demonstrated over the past few years, the creation of such vibro-polaritons allows the manipulation of molecular processes occurring at the electronic ground-state, by targeting a specific intra-molecular bond and coupling its associated vibration to an optical mode^{18,37,38}.

A different class of vibrational modes in organic materials are inter-molecular vibrations, which are particularly relevant in large molecular structures such as organic crystalline materials, polymers, and proteins. These vibrations, which typically lie in the terahertz frequency regime (10^{11} – 10^{13} Hz, or several tens of cm^{-1}), correspond to the concerted motion of the unit cells, one with respect to another (rather than internal vibrations of atoms within each molecule). Moreover, these collective vibrations are extended over many inter-molecular bonds. Here, we demonstrate strong coupling of collective vibrations in ensembles of organic α -lactose molecules, occurring at 0.53 THz. Unlike the previously studied vibrational strong coupling, here the cavity mode is coupled to the inter-molecular vibration extended over the crystallites, i.e. the oscillatory motion of the hydrogen-bonded molecules with respect to one another. We observe the Rabi-splitting typical of strong coupling and coherent Rabi-oscillations at room temperature, despite the fact that the energy of the collective vibrational transition ($\hbar\nu_{\text{vib}} \sim 2$ meV), as well as the light-matter interaction strength, are much lower than $k_{\text{B}}T$ (~ 25 meV). Our results extend the applicability of polaritonic chemistry to a plethora of large-scale organic systems, such as biological macromolecules³⁹, polymer chains⁴⁰, energetic materials with low lying collective vibrations⁴¹, skeletal motions in metal organic frameworks (MOFs)⁴², and many others.

Results

Hybrid cavity-lactose system. Lactose is a disaccharide composed of galactose and glucose, and it is one of the primary ingredients of milk. In this study we use α -lactose monohydrate, which is one of the anomers formed upon the crystallization of lactose, with the chemical structure shown in Fig. 1a. The α -lactose powder used in this study (as purchased from Sigma-Aldrich) is comprised of small, polycrystalline particles, a few tens

of microns in size, as shown in Fig. 1b. To measure its THz absorption spectrum, we prepared a ~ 1.3 -mm-thick pellet of pristine α -lactose using a pressing die (see Methods section), and measured its absorption spectrum using terahertz time-domain spectroscopy (THz-TDS). From this measurement we obtain the frequency-dependent absorption coefficient, which is given by $\alpha(\nu) = \ln(10)A/l$ with A being the absorption spectrum and l the pellet thickness. The result is presented in Fig. 1c, showing a sharp absorption peak at 0.53 THz (17.7 cm^{-1}) with a width of 21 GHz full-width half-maximum (FWHM). This absorption line corresponds to a collective, intermolecular vibration in the molecular crystal, in which the molecules move with respect to each other as a rigid body^{43–45}. An additional weaker absorption peak is observed within our usable THz bandwidth, at 1.2 THz. In order to demonstrate strong coupling of the collective vibrational mode at 0.53 THz, we utilized the open-cavity geometry⁴⁶ depicted in Fig. 1d (see Methods section for further details). The cavity is composed of two Au mirrors prepared by sputtering ~ 6 nm Au layers on 1-mm-thick quartz substrates. The reflection amplitude of the mirrors was measured to be $\sim 90\%$ for the THz field (81% reflectivity). In the open cavity geometry, one of the mirrors is fixed, while the other is mounted on a computer-controlled translation stage, parallel to the fixed mirror, such that the cavity length d can be varied continuously.

Terahertz spectroscopy measurements. The measurements were performed using a home-built, time-domain terahertz spectrometer, shown in the schematic diagram in Fig. 2a. In a typical measurement, an ultrashort laser pulse (100 fs pulse duration, 800 nm central wavelength) from a Ti:Sapphire chirped pulse amplifier (Legend Duo, Coherent Inc.) is split to form a strong optical beam for THz generation and a weak readout pulse for time-resolved electro-optic sampling of the THz field^{47,48}. A single-cycle THz pulse is generated via tilted pulse-front optical rectification in LiNbO_3 (LN)⁴⁹ and focused through the sample (S), which is placed at the focal plane of a 4-f setup composed of two off-axis parabolic reflectors. The THz field and the readout pulse are combined by a pellicle beam-splitter (PBS) and focused at the electro-optic detection crystal (Gallium Phosphate, GaP), following which the probe beam is analyzed for its differential polarization changes (by splitting the two polarizations with a Wollaston Prism [WP] and a pair of photodiodes [PD]). The signals are detected using a lock-in amplifier (Stanford Research Systems, SR830) and recorded by a desktop PC. The peak field strength of the THz pulse is ~ 50 kV/cm. The entire system is purged with dry air (relative humidity $< 4\%$) to eliminate THz absorption by the water vapor in the ambient lab atmosphere (water absorption lines of 0.56, 0.75, and 0.98 THz are clearly observed in our THz spectrum and are completely removed when the system is purged with dry air). Also shown in Fig. 2 are the measured electric field of the generated THz pulse (Fig. 2b) and its calculated power spectrum (Fig. 2c). As seen, the input field is indeed a single-cycle pulse, centered around 0.6 THz with a usable spectrum covering the 0.1–1.2 THz range.

First, we characterized the response of the empty cavity, i.e., when the gap between the mirrors contains only dry air. Note that in such time-domain experiments, parasitic reflections within the THz-TDS spectrometer result in spurious signals which enter the measurements. As detailed in Supplementary Note 1, we deconvolute the raw signal from the instrument response function to eliminate these distortions^{50,51}. The results of the THz-TDS (following deconvolution) are presented in Fig. 3a, showing the time-domain signal of the field exiting the cavity, for several different cavity length values (at normal incidence). As can be seen, when the single-cycle THz pulse passes through the

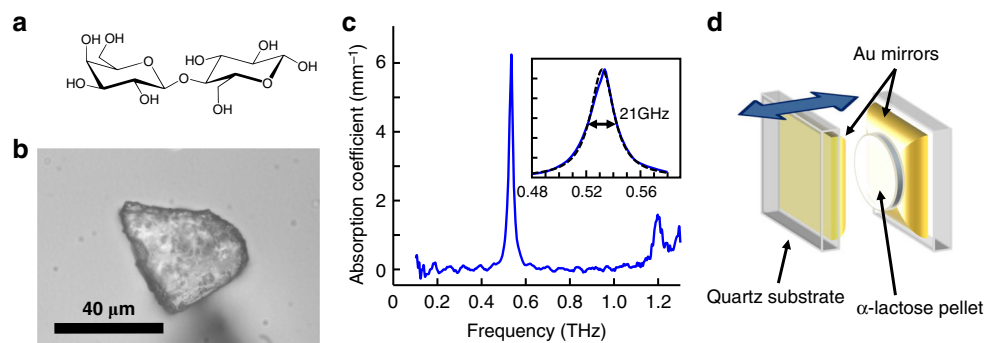


Fig. 1 α -Lactose molecules in a tunable THz cavity. **a** Chemical structure of α -lactose. **b** A microscope image of an α -lactose crystallite. **c** Absorption coefficient of the α -lactose pellet obtained from the THz absorption measurement. The inset shows the fit of the measured absorption peak (blue line) to a lorentzian line-shape (black dashed line). **d** A sketch of the open THz cavity used in the experiments

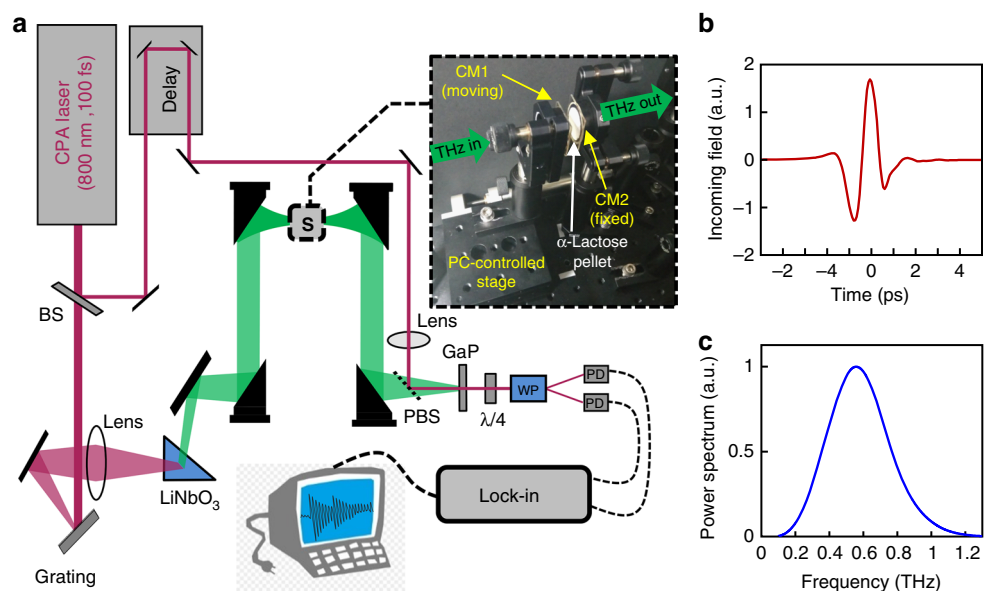


Fig. 2 Time-domain THz spectrometer. **a** Schematic sketch of the optical setup. The inset shows a photograph of the open cavity, which is formed by a moveable mirror (CM1) and a fixed mirror (CM2). **b** The time-resolved single-cycle THz field used in this work and **c** its power spectrum, obtained by the Fourier transform of the data in **b**

cavity, it is stretched to an exponentially decaying oscillatory signal, as expected for a resonant cavity with a finite lifetime. The transmission spectrum of the cavity can then be calculated by taking the ratio between the power spectra of the (deconvoluted) transmitted signals shown in Fig. 3a and dividing them by the input pulse power spectrum, shown in Fig. 2c. These transmission spectra, calculated for the different cavity lengths, are shown in Fig. 3b. As can be seen, the resonant Fabry–Pérot cavity modes are clearly visible, with their frequencies obeying the relation $f_m = \frac{c}{2d}m$, where c is the speed of light, d is the cavity length (the distance between the mirrors), and m is the mode number (assigned in Fig. 3b). Specifically, for a cavity length of 640 μm , for which the second-order mode is close to the α -lactose absorption line, the resonant modes have a transmission peak of 0.5–1% and a linewidth of ~ 14 GHz, matching the calculated finesse for mirrors with reflectivity of 81%. In addition, we performed transfer-matrix calculations (see Methods section) for the 640 μm cavity to simulate the spectral response of the cavity (solid green line in Fig. 3b), which agree with the experimental measurement.

Next, we examined the response of the cavity with the α -lactose pellet placed between the mirrors. We prepared an α -lactose

pellet of 250 μm in thickness, attached it to the fixed mirror and adjusted the total cavity length to ~ 350 μm . Under such conditions, the effective optical length of the cavity (given by $d_{\text{opt}} = d_{\text{al}}n_{\text{al}} + d_{\text{air}}$ with d_{al} being the pellet thickness, $n_{\text{al}} = 1.8$ the background refractive index of α -lactose⁵², and $d_{\text{air}} \sim 100$ μm is the thickness of the air-gap) is ~ 550 μm , such that the second-order cavity mode is resonant with the collective vibrational mode of the α -lactose at 0.53 THz. We note that we chose to target the second-order mode of the cavity since tuning the first cavity mode to 0.53 THz would require a thinner α -lactose pellet (~ 150 μm), which results in fragility and inhomogeneity of the pellet. The time-resolved THz field exiting the cavity is presented in Fig. 4a. We observe a similar exponentially decaying oscillation, as in the empty cavities, but here the signal is modulated by a periodic envelope. This periodic modulation corresponds to Rabi-oscillations in the cavity—an excitation that is shared by both the photonic cavity and the inter-molecular vibration of the α -lactose, serving as an indication of the strong coupling between those two entities^{1,2,53}. The transmission spectrum of the α -lactose cavity, obtained using the Fourier transform of the signal in Fig. 4a, is shown in Fig. 4b (blue solid line). Furthermore, by fitting the results to transfer-matrix calculations (using the experimentally

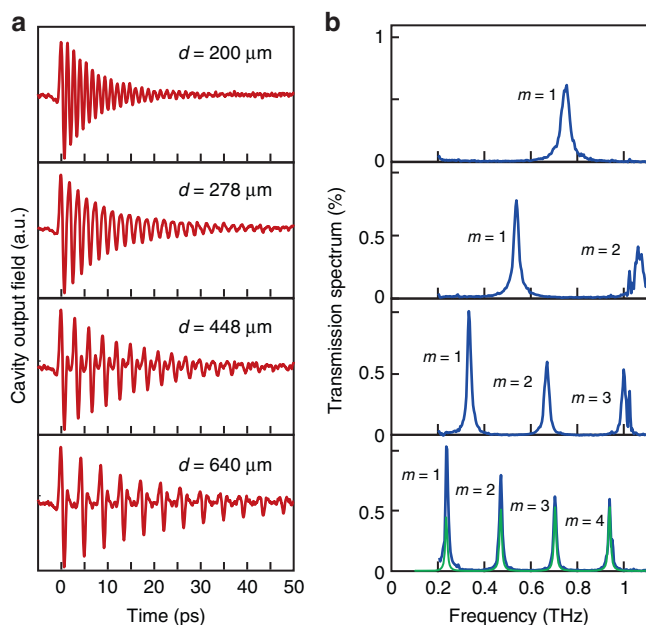


Fig. 3 Time-domain THz spectroscopy of an empty cavity. **a** Time-resolved THz signal measured at the output of the empty cavity with different distances, d , between the mirrors, showing the exponentially decaying oscillations of the field exiting the cavity. **b** Transmission power spectra of the cavity with increasing cavity lengths, showing the gradual progression of the empty-cavity resonant modes. The green line shows the transmission spectrum obtained by T -matrix calculations

measured refractive index of α -lactose⁵²), shown by the green solid line, we obtain a thickness of $d_{\text{al}} = 250 \mu\text{m}$ for the α -lactose pellet and $d_{\text{air}} = 97 \mu\text{m}$ for the air gap thickness. As can be seen in both the experimental measurement and the simulations, the hybrid cavity/ α -lactose system exhibits a clear splitting in the spectral response around the collective vibration frequency and the formation of two THz vibro-polariton states, at 0.50 and 0.56 THz, indicating once again that the hybrid system is indeed within the strong coupling regime. In addition to the polaritonic modes, the first ($m = 1$)- and third ($m = 3$)-order cavity modes at 0.25 and 0.83 THz are also located within the bandwidth of the input pulse. Therefore, the single-cycle pulse excites a coherent superposition of the polaritonic modes as well as the non-coupled cavity modes, which gives rise to the seemingly irregular dynamics seen in the time domain (Fig. 4a). To illustrate this, we numerically filter the time-domain signal by a band-pass filter, leaving only frequencies within the range of 0.38–0.68 THz. The filtered time-domain signal is presented in Fig. 4c. As seen, the Rabi-oscillations of the coupled system are clearly observed, demonstrating the reversible and coherent light-matter interaction taking place in the system. Interestingly, Rabi oscillations occurring under strong coupling of molecular excitons and plasmonic structures were previously observed by probing the excited state population, using ultrafast pump-probe spectroscopy⁵³. However, here we are able to observe the Rabi-oscillations in the emitted field directly, including its oscillating phase. It is important to note that the Rabi splitting observed in our experiment (as also in other polaritonic systems) is not induced by the THz pulse itself. Instead, the THz field merely probes the coupled states of the system, which are formed by the interaction of the molecular vibrations with the cavity mode^{1,14}. This is also evident by the fact that the spectral response of the coupled cavity (shown in Fig. 4b) does not change when the intensity of the THz pulse is varied (see Supplementary Note 2).

Vibro-polariton dispersion. Next, we varied the position of the moveable mirror, repeated the measurement, and calculated the spectral response as shown in Fig. 4b, for several different cavity lengths. As shown in Fig. 4d (blue lines), when the cavity is detuned from the vibrational absorption peak, the frequencies of the polaritonic modes are shifted relative to the resonant case, and the relative strengths of their transmission peaks also changes. As expected, in the time domain (see Supplementary Fig. 5) these features are manifested by a lower modulation depth of the Rabi oscillations and a shorter Rabi cycle for the oscillating envelope, as compared to Fig. 4c. Also shown in Fig. 4d are the simulated transfer-matrix results for the coupled system (green lines, see Methods section for further details). In our simulations, we fix all the parameters except for the thickness of the air-gap between the pellet surface and the moveable mirror, which is extracted by fitting the simulated transmission spectrum to the experimental data (note that the transfer-matrix formalism provides the linear spectral response of the cavity, thus the excellent agreement between the experimental and the simulated transmission data further indicates that the THz field only serves as a probe for the resonances of the coupled system and does not govern the strong-coupling effect, as also verified experimentally in Supplementary Note 2). Using these simulations, we can extract the second-order cavity resonance for each value of the cavity thickness, by removing the contribution of the vibrational resonance to the refractive index of the α -lactose, only taking into account its background index of refraction. Finally, we use these results to plot the dispersion of the hybrid molecular/cavity system, i.e. the measured vibro-polariton frequencies as a function of the cavity resonance frequency. As seen in Fig. 5, the dispersion shows the formation of the characteristic polariton branches around the absorption frequency of the α -lactose collective vibration. We fit these measurements to the dispersion resulting from the coupled-oscillator model, which gives the real part of the resonance frequencies of the coupled system as⁵⁴

$$\nu_{\pm} = \frac{\nu_c + \nu_{\text{vib}}}{2} \pm \sqrt{(V/h)^2 + \frac{1}{4} \left[(\nu_c - \nu_{\text{vib}}) - \frac{i}{2} (\gamma_c - \gamma_{\text{vib}}) \right]^2}, \quad (1)$$

where V is the dipolar light-matter interaction energy (see Methods section for further details), h is Planck's constant, $\nu_{\text{vib}} = 0.53 \text{ THz}$ is the collective vibration frequency, ν_c is the cavity frequency (of the second-order mode), and $\gamma_{\text{vib}} = 21 \text{ GHz}$ and $\gamma_c = 14 \text{ GHz}$ are their FWHM linewidths. At resonance ($\nu_c = \nu_{\text{vib}}$), the difference between the two polaritonic frequencies gives the Rabi frequency of the couple system $\nu_R = 2\sqrt{(V/h)^2 - \frac{1}{16}(\gamma_c - \gamma_{\text{vib}})^2}$. By fitting Eq. (1) to the measured data, we obtain a Rabi frequency value of $\nu_R = 68 \text{ GHz}$, which also reflects the coupling energy $V = h\nu_R$ under the experimental conditions (since $\gamma_c - \gamma_{\text{vib}} \ll \nu_R$). This value satisfies the condition $\nu_R > \frac{\gamma_c - \gamma_{\text{vib}}}{2}$, confirming that our system is indeed within the coherent, strong coupling regime¹⁴. Moreover, this Rabi splitting value is about 13% of the bare vibration frequency, placing this system close to the ultrastrong coupling regime.

Discussion

We have demonstrated the strong-coupling of the collective vibration of α -lactose crystallites and a Fabry-Pérot cavity in the low-THz frequency region (0.53 THz), and observed a Rabi-splitting of $\sim 13\%$ of the fundamental frequency. Moreover, we have observed the coherent vacuum Rabi-oscillations taking place in the coupled system, taking advantage of the ability to perform

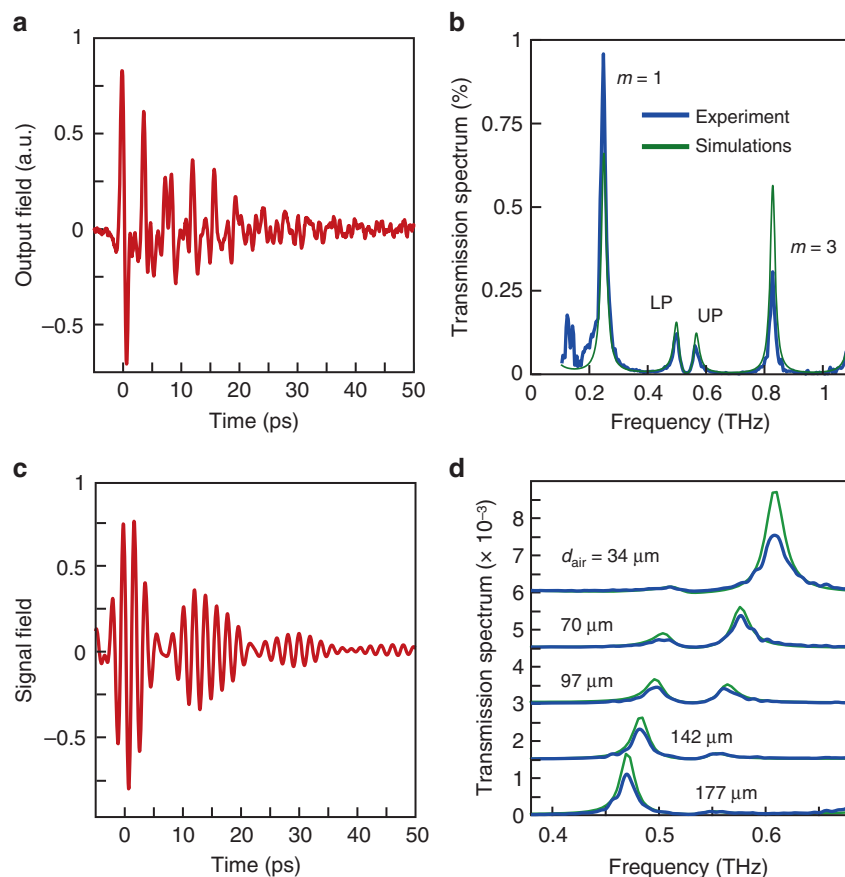


Fig. 4 Strong coupling of collective THz vibrations in α -lactose. **a** Measured time-domain output signal from the cavity with the α -lactose pellet, with its length chosen such that the second cavity resonance ($m = 2$) is at 0.53 THz. **b** Transmission spectrum of the cavity with α -lactose with a total cavity length of 350 μm , obtained from the experimentally measured time domain signal in Fig. 4a (blue line) and by T-matrix calculations (green line). The strong coupling between the collective vibrations and the cavity results in a spectral splitting that indicates the formation of hybrid vibro-polariton states. **c** Spectrally filtered output signal from the cavity, showing the Rabi-oscillations of the coupled system in the time-domain. **d** Selected cavity transmission spectra in the vicinity of the α -lactose absorption peak (0.53 THz), measured with different air gap thicknesses d_{air} and α -lactose pellet thickness of $d_{\text{al}} = 250 \mu\text{m}$ (blue lines), compared to T-matrix calculations (green lines)

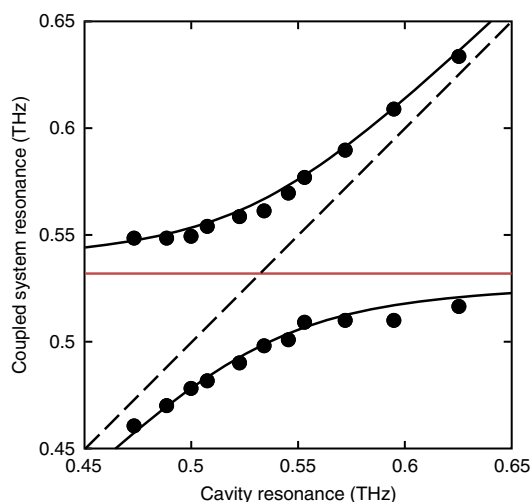


Fig. 5 THz vibro-polariton branches of strongly coupled α -lactose. The circles correspond to the measured polariton peaks, which were obtained by scanning the cavity resonance across the α -lactose absorption (marked by the horizontal red line). The dashed black line marks the empty cavity resonance while the solid black curves show the result of the coupled oscillator model (Eq. (1)) fitted to the measured data

time-domain and phase-sensitive measurements of the THz field. Interestingly, since the measurements are performed at room temperature, the energy of the collective vibration $h\nu_{\text{vib}} = 2.2 \text{ meV}$ and the Rabi-splitting energy $h\nu_{\text{R}} = 0.28 \text{ meV}$ are both lower than $k_{\text{B}}T$. This places our system in a very different regime than all previously studied organic strong-coupled systems, and expected to result in a different coupling to the surrounding thermal bath and therefore different relaxation dynamics⁵⁵.

Finally, in contrast to previous works that studied vibrational strong coupling with intra-molecular vibrations or phonons in inorganic crystals, where covalent bonds were strongly coupled to the photonic modes, here we strongly couple the hydrogen bonds by which the molecules are held together. Such weak hydrogen bonds, whose vibrational frequencies often reside in the THz range³⁹, are central to supramolecular chemistry and biological functionality. In the context of polaritonic chemistry, the ability to affect these weak bonds by modifying their collective vibrational modes may be used to judiciously control chemical and biological processes that depend on extended degrees of freedom. For example, collective THz vibrational excitations are involved in the conformational changes and binding events in proteins^{56–58}, and therefore modifying the natural vibrational modes by strong coupling is expected to alter the biological functionality of proteins, in a similar manner to heavy element substitution³⁶. Furthermore, many biological processes are

governed by the collective low-frequency vibrations of the surrounding hydrogen-bonded water network⁵⁹, which may also be affected by strong coupling. Going beyond biology, the mechanical and morphological properties of polymers and organic crystals are intimately linked to THz-active vibrations of the inter-molecular hydrogen bonds^{42,60,61}, and in various chemical processes, such as detonation in energetic materials, mechanical energy on the macroscopic scale is funneled through collective THz modes into intra-molecular bonds, to drive the chemical reaction⁶². In such systems, as well as others, strong coupling between collective THz vibrations and an optical resonator may be used to manipulate the material properties and reaction pathways.

The relatively easy fabrication of the open-mirror-cavity demonstrated here, together with the direct measurement of the amplitude and phase of the electric field in time-domain THz spectroscopy, provide an extended test-bed for studying the very basic underlying physics of the strong-coupling phenomenon. Furthermore, the relatively large (tens to hundreds of μm) length-scale of the THz cavity makes it accessible to additional stimulations, such as optical excitations, that may alter the molecular structure, as well as to structural patterning of the sample to manipulate the light-matter interaction within cavity.

Methods

Open cavity configuration. The variable-length open cavity used in this work (see Fig. 2) is composed of a moveable mirror (CM1) and a fixed mirror (CM2). Both mirrors were produced by sputtering a thin layer (6 nm) of gold on a quartz substrate (1 mm thickness), resulting in a transmission amplitude of 90% across the whole usable bandwidth with no apparent spectral dependence. CM1 is mounted on a computer-controlled single-axis stage, with micrometer resolution ($<2\ \mu\text{m}$ repeatability). By moving CM1 with respect to CM2 we control the length of the cavity and corresponding resonance frequency. CM1 and CM2 are set parallel to each other by coinciding the multiple reflections of a green diode laser from the mirrors at the far field. The α -lactose sample (white, round pellet) was prepared by placing 0.1 g of α -Lactose powder in a pressing die (20 mm diameter) at a pressure of 220 kN for 10 min, which yielded a $\sim 250\ \mu\text{m}$ pellet. The pellet was then glued onto CM2 at a few points around its circumference.

Transfer matrix calculations. The simulated transmission spectra of the cavity were calculated using the transfer-matrix formalism, which provides the linear transmission spectrum of the cavity (with and without the α -lactose) by solving the wave propagation through the multilayer structure^{35,63}. In these simulations, we used the experimentally measured refractive index of gold⁶⁴ to model the cavity mirrors and adjusted the thickness of the mirrors to match the measured reflectivity of 81%. We note that the fitted thickness of the mirrors was found to be 1.5 nm, which is lower than the actual thickness of 6 nm. This is most probably due to the fact that at such low thicknesses the sputtered metal film is not continuous, but rather composed of small Au islands. The interaction with the molecules can be modeled classically by including their frequency-dependent complex dielectric function in the transfer-matrix simulations^{14,35,54,65}. Within our usable THz range, the dielectric function of the α -lactose pellet is accurately described by a Lorentz-Drude model with contributions from three different vibrational transitions⁵²

$$\epsilon_{\text{al}}(\nu) = \epsilon_0 \left[\epsilon_{\infty} + \sum_{i=1}^3 \frac{\nu_{\text{p},i}^2}{\nu_i^2 - \nu^2 - i\gamma_i\nu} \right], \quad (2)$$

where ϵ_0 is the vacuum permittivity, $\epsilon_{\infty} = 3.2$ is the (relative) background dielectric constant, $\nu_i = 0.53, 1.195, \text{ and } 1.37\ \text{THz}$ are the vibrational frequencies, $\gamma_i = 21, 44, \text{ and } 58\ \text{GHz}$ are the linewidths, and $\nu_{\text{p},i} = 0.123, 0.072, \text{ and } 0.253\ \text{THz}$ are the corresponding plasma frequencies.

Microscopic estimation of the Rabi frequency. The vacuum Rabi frequency is related to the collective dipolar coupling between the optical transition in the molecules and the field contributed by a single photon in the cavity^{1,14}, given by $V = d\sqrt{\frac{h\nu}{2\epsilon_0\epsilon_{\infty}V_c}N}$ with d being the transition dipole element of each molecule, h is the Planck constant, ν is the cavity resonance frequency (taken as equal to the vibrational transition frequency of 0.53 THz), ϵ_{∞} is the background dielectric constant inside the cavity, V_c is the cavity mode volume, and N the number of molecules (or number of resonant vibrating bonds, in the case of vibrational strong coupling). Under resonant conditions (Fig. 4a–c) the lactose pellet almost fills the entire gap between the mirrors. For metallic cavities under such conditions, the volume occupied by the molecules can be approximately taken as the mode

volume⁶⁶, such that the ratio N/V_c can be roughly taken as the molecular concentration. With a molar weight of $342\ \text{g mol}^{-1}$ and a density of $1.52\ \text{g cm}^{-3}$, this concentration is $n = 2.6 \times 10^{21}\ \text{cm}^{-3}$. In our system, the cavity mode is coupled to a collective vibration, which is extended across many molecules and therefore the coupling needs to be described in terms of a collective transition dipole operator, in a similar manner to ref. 35. However, one may define an effective molecular transition dipole, which can be extracted from the absorption spectrum shown in Fig. 1c while treating the molecules as individual absorbers. Using the relation $d^2 = \frac{3\epsilon_0\hbar c}{2\pi^2\nu} \Delta\nu\sigma_{\text{abs}}$ (where ϵ_0 is the dielectric constant of vacuum, c the speed of light, ν the transition frequency, $\Delta\nu$ the absorption linewidth, and σ_{abs} is the absorption cross section⁶⁷) and taking $\sigma_{\text{abs}} = \alpha/n$ with the measured absorption coefficient $\alpha = 6.3\ \text{mm}^{-1}$ at the 0.53 THz line, we obtain a transition dipole element of $d = 0.06$ Debye. Using this value and $\epsilon_{\infty} = 3.2$, the expected coupling energy is $V = 0.16\ \text{meV}$. This corresponds to a Rabi frequency of $2V/\hbar = 76\ \text{GHz}$, in very good agreement with our experimental observation.

Data Availability

The data that support the findings of this study are available from the corresponding author upon reasonable request.

Received: 7 January 2019 Accepted: 18 June 2019

Published online: 19 July 2019

References

- Ebbesen, T. W. Hybrid light–matter states in a molecular and material science perspective. *Acc. Chem. Res.* **49**, 2403–2412 (2016).
- Kaluzny, Y., Goy, P., Gross, M., Raimond, J. & Haroche, S. Observation of self-induced Rabi oscillations in two-level atoms excited inside a resonant cavity: the ringing regime of superradiance. *Phys. Rev. Lett.* **51**, 1175–1178 (1983).
- Raizen, M. G., Thompson, R. J., Brecha, R. J., Kimble, H. J. & Carmichael, H. J. Normal-mode splitting and linewidth averaging for two-state atoms in an optical cavity. *Phys. Rev. Lett.* **63**, 240–243 (1989).
- Thompson, R. J., Rempe, G. & Kimble, H. J. Observation of normal-mode splitting for an atom in an optical cavity. *Phys. Rev. Lett.* **68**, 1132–1135 (1992).
- Weisbuch, C., Nishioka, M., Ishikawa, A. & Arakawa, Y. Observation of the coupled exciton-photon mode splitting in a semiconductor quantum microcavity. *Phys. Rev. Lett.* **69**, 3314–3317 (1992).
- Khitrova, G. et al. Vacuum Rabi splitting in semiconductors. *Nat. Phys.* **2**, 81–90 (2006).
- Kubo, Y. et al. Strong coupling of a spin ensemble to a superconducting resonator. *Phys. Rev. Lett.* **105**, 1–4 (2010).
- Shelton, D. J. et al. Strong coupling between nanoscale metamaterials and phonons. *Nano Lett.* **11**, 2104–2108 (2011).
- Luxmoore, I. J. et al. Strong coupling in the far-infrared between graphene plasmons and the surface optical phonons of silicon dioxide. *ACS Photonics* **1**, 1151–1155 (2014).
- Jin, X. et al. Reshaping the phonon energy landscape of nanocrystals inside a terahertz plasmonic nanocavity. *Nat. Commun.* **9**, 763 (2018).
- Sivarajah, P. et al. THz-frequency magnon-phonon-polaritons in the collective strong-coupling regime. *J. Appl. Phys.* **125**, 213103 (2019).
- Pockrand, I., Brillante, A. & Mobius, D. Introduction, I. Exciton-surface plasmon coupling: an experimental investigation. *J. Chem. Phys.* **77**, 6289–6295 (1982).
- Lidzey, D. G. et al. Strong exciton-photon coupling in an organic semiconductor microcavity. *Nature* **395**, 53–55 (1998).
- Törmä, P. & Barnes, W. L. Strong coupling between surface plasmon polaritons and emitters: a review. *Rep. Prog. Phys.* **78**, 013901 (2015).
- Flick, J., Ruggenthaler, M., Appel, H. & Rubio, A. Atoms and molecules in cavities, from weak to strong coupling in quantum-electrodynamics (QED) chemistry. *Proc. Natl. Acad. Sci. USA* **114**, 3026–3034 (2017).
- Feist, J., Galego, J. & Garcia-Vidal, F. J. Polaritonic chemistry with organic molecules. *ACS Photonics* **5**, 205–216 (2018).
- Hutchison, J. A., Schwartz, T., Genet, C., Devaux, E. & Ebbesen, T. W. Modifying chemical landscapes by coupling to vacuum fields. *Angew Chem. Int. Ed.* **51**, 1592–1596 (2012).
- Thomas, A. Ground-state chemical reactivity under vibrational coupling to the vacuum electromagnetic field. *Angew Chem. Int. Ed.* **55**, 11462–11466 (2016).
- Galego, J., Garcia-Vidal, F. J. & Feist, J. Suppressing photochemical reactions with quantized light fields. *Nat. Commun.* **7**, 13841 (2016).
- Herrera, F. & Spano, F. C. Cavity-controlled chemistry in molecular ensembles. *Phys. Rev. Lett.* **116**, 238301 (2016).
- Groenhof, G. & Toppari, J. J. Coherent light harvesting through strong coupling to confined light. *J. Phys. Chem. Lett.* **9**, 4848–4851 (2018).

22. Munkhbat, B., Wersäll, M., Baranov, D. G., Antosiewicz, T. J. & Shegai, T. Suppression of photo-oxidation of organic chromophores by strong coupling to plasmonic nanoantennas. *Sci. Adv.* **4**, eaas9552 (2018).
23. Wang, S. et al. Quantum yield of polariton emission from hybrid light-matter states. *J. Phys. Chem. Lett.* **5**, 1433–1439 (2014).
24. Ballarini, D. et al. Polariton-induced enhanced emission from an organic dye under the strong coupling regime. *Adv. Opt. Mater.* **2**, 1076–1081 (2014).
25. Stranius, K., Hertzog, M. & Börjesson, K. Selective manipulation of electronically excited states through strong light-matter interactions. *Nat. Commun.* **9**, 2273 (2018).
26. Orgiu, E. et al. Conductivity in organic semiconductors hybridized with the vacuum field. *Nat. Mater.* **14**, 1123–1129 (2015).
27. Feist, J. & Garcia-Vidal, F. J. Extraordinary exciton conductance induced by strong coupling. *Phys. Rev. Lett.* **114**, 196402 (2015).
28. Schachenmayer, J., Genes, C., Tignone, E. & Pupillo, G. Cavity-enhanced transport of excitons. *Phys. Rev. Lett.* **114**, 196403 (2015).
29. Hagenmüller, D., Schachenmayer, J., Schütz, S., Genes, C. & Pupillo, G. Cavity-enhanced transport of charge. *Phys. Rev. Lett.* **119**, 223601 (2017).
30. Rozenman, G. G., Akulov, K., Golombek, A. & Schwartz, T. Long-range transport of organic exciton-polaritons revealed by ultrafast microscopy. *ACS Photonics* **5**, 105–110 (2018).
31. Shalabney, A. et al. Coherent coupling of molecular resonators with a microcavity mode. *Nat. Commun.* **6**, 5981 (2015).
32. Long, J. P. & Simpkins, B. S. Coherent coupling between a molecular vibration and Fabry-Perot optical cavity to give hybridized states in the strong coupling limit. *ACS Photonics* **2**, 130–136 (2015).
33. George, J., Shalabney, A., Hutchison, J. A., Genet, C. & Ebbesen, T. W. Liquid-phase vibrational strong coupling. *J. Phys. Chem. Lett.* **6**, 1027–1031 (2015).
34. Muallem, M., Palatnik, A., Nessim, G. D. & Tischler, Y. R. Strong light-matter coupling and hybridization of molecular vibrations in a low-loss infrared microcavity. *J. Phys. Chem. Lett.* **7**, 2002–2008 (2016).
35. George, J. et al. Multiple Rabi splittings under ultrastrong vibrational coupling. *Phys. Rev. Lett.* **117**, 153601 (2016).
36. Vergauwe, R. M. A. et al. Quantum strong coupling with protein vibrational modes. *J. Phys. Chem. Lett.* **7**, 4159–4164 (2016).
37. Thomas, A. et al. Tilting a ground-state reactivity landscape by vibrational strong coupling. *Science* **363**, 615–619 (2019).
38. Hiura, H., et al. Cavity catalysis—accelerating reactions under vibrational strong coupling. Preprint at <https://doi.org/10.26434/chemrxiv.7234721.v3> (2018).
39. Plusquellic, D. F., Siegrist, K., Heilweil, E. J. & Esenturk, O. Applications of terahertz spectroscopy in biosystems. *ChemPhysChem* **8**, 2412–2431 (2007).
40. Wietzke, S. et al. Terahertz spectroscopy on polymers: a review of morphological studies. *J. Mol. Struct.* **1006**, 41–51 (2011).
41. Davies, A. G., Burnett, A. D., Fan, W., Linfield, E. H. & Cunningham, J. E. Terahertz spectroscopy of explosives and drugs. *Mater Today* **11**, 18–26 (2008).
42. Ryder, M. R., Civalleri, B., Cinque, G. & Tan, J.-C. Discovering connections between terahertz vibrations and elasticity underpinning the collective dynamics of the HKUST-1 metal-organic framework. *CrystEngComm* **18**, 4303–4312 (2016).
43. Brown, E. R., Bjarnason, J. E., Fedor, A. M. & Kortner, T. M. On the strong and narrow absorption signature in lactose at 0.53THz. *Appl. Phys. Lett.* **90**, 061908 (2007).
44. Allis, D. G., Fedor, A. M., Kortner, T. M., Bjarnason, J. E. & Brown, E. R. Assignment of the lowest-lying THz absorption signatures in biotin and lactose monohydrate by solid-state density functional theory. *Chem. Phys. Lett.* **440**, 203–209 (2007).
45. Jin, B. B., et al. Mode assignment of terahertz spectrum of α -lactose monohydrate. In *2009 34th International Conference on Infrared, Millimeter, and Terahertz Waves 1–2* (IEEE, 2009, Busan, South Korea). <https://ieeexplore.ieee.org/document/5324682>.
46. Kapon, O., Yitzhari, R., Palatnik, A. & Tischler, Y. R. Vibrational strong light-matter coupling using a wavelength-tunable mid-infrared open microcavity. *J. Phys. Chem. C* **121**, 18845–18853 (2017).
47. Wu, Q. & Zhang, X. C. Free-space electro-optic sampling of terahertz beams. *Appl. Phys. Lett.* **67**, 3523 (1995).
48. Nahata, A., Weling, A. S. & Heinz, T. F. A wideband coherent terahertz spectroscopy system using optical rectification and electro-optic sampling. *Appl. Phys. Lett.* **69**, 2321–2323 (1996).
49. Yeh, K.-L., Hoffmann, M. C., Hebling, J. & Nelson, K. A. Generation of 10 μ J ultrashort terahertz pulses by optical rectification. *Appl. Phys. Lett.* **90**, 171121 (2007).
50. Damari, R., Kallush, S. & Fleischer, S. Rotational control of asymmetric molecules: dipole- versus polarizability-driven rotational dynamics. *Phys. Rev. Lett.* **117**, 103001 (2016).
51. Damari, R., Rosenberg, D. & Fleischer, S. Coherent radiative decay of molecular rotations: a comparative study of terahertz-oriented versus optically aligned molecular ensembles. *Phys. Rev. Lett.* **119**, 033002 (2017).
52. Roggenbuck, A. et al. Coherent broadband continuous-wave terahertz spectroscopy on solid-state samples. *New J. Phys.* **12**, 043017 (2010).
53. Vasa, P. et al. Real-time observation of ultrafast Rabi oscillations between excitons and plasmons in metal nanostructures with J-aggregates. *Nat. Photonics* **7**, 128–132 (2013).
54. Savona, V., Andreani, L. C., Schwendimann, P. & Quattropani, A. Quantum well excitons in semiconductor microcavities: unified treatment of weak and strong coupling regimes. *Solid State Commun.* **93**, 733–739 (1995).
55. Pino, J., del Feist, J. & Garcia-Vidal, F. J. Quantum theory of collective strong coupling of molecular vibrations with a microcavity mode. *New J. Phys.* **17**, 053040 (2015).
56. Deák, J., Chiu, H.-L., Lewis, C. M. & Miller, R. J. D. Ultrafast phase grating studies of heme proteins: observation of the low-frequency modes directing functionally important protein motions. *J. Phys. Chem. B* **102**, 6621–6634 (1998).
57. Turton, D. A. et al. Terahertz underdamped vibrational motion governs protein-ligand binding in solution. *Nat. Commun.* **5**, 3999 (2014).
58. Niessen, K. A. et al. Moving in the right direction: protein vibrations steering function. *Biophys. J.* **112**, 933–942 (2017).
59. Grossman, M. et al. Correlated structural kinetics and retarded solvent dynamics at the metalloprotease active site. *Nat. Struct. Mol. Biol.* **18**, 1102–1108 (2011).
60. Hoshina, H. et al. Polymer morphological change induced by terahertz irradiation. *Sci. Rep.* **6**, 27180 (2016).
61. Ruggiero, M. T., Axel Zeitler, J. & Kortner, T. M. Concomitant polymorphism and the martensitic-like transformation of an organic crystal. *Phys. Chem. Chem. Phys.* **19**, 28502–28506 (2017).
62. Dlott, D. D. & Fayer, M. D. Shocked molecular solids: vibrational up pumping, defect hot spot formation, and the onset of chemistry. *J. Chem. Phys.* **92**, 3798–3812 (1990).
63. Yeh, P. *Optical Waves in Layered Media* (Wiley, 2005).
64. Yasuda, H. & Hosako, I. Measurement of terahertz refractive index of metal with terahertz time-domain spectroscopy. *Jpn J. Appl. Phys.* **47**, 1632–1634 (2008).
65. Bradley, M., Tischler, J., Shirasaki, Y. & Bulović, V. Predicting the linear optical response of J-aggregate microcavity exciton-polariton devices. *Phys. Rev. B* **78**, 4–7 (2008).
66. Hobson, P. A. et al. Strong exciton-photon coupling in a low-Q all-metal mirror microcavity. *Appl. Phys. Lett.* **81**, 3519–3521 (2002).
67. Demtröder, W. *Laser Spectroscopy* (Springer, Berlin, Heidelberg, 2008).

Acknowledgements

We thank C. Genet for the useful discussions. This work was supported by the Wolfson Foundation Grant No. PR/ec/20419. S.F. acknowledges the support of the Israel Science Foundation (ISF), Grants No. 1065/14, No. 926/18, Grant No. 2797/11 (INREP—Israel National Research Center for Electrochemical Propulsion) and the Wolfson Foundation Grant No. PR/eh/21797. T.S. acknowledges the support of the ISF Grant No. 1241/13. K.A. acknowledges the financial support from the Ministry of Science and Technology, Israel.

Author Contributions

T.S. and S.F. conceived the experiment, supervised the project, and co-wrote the paper. R.D., O.W., and D.K. performed the THz spectroscopy measurements. All authors contributed equally to the sample design and fabrication and to the data analysis.

Additional information

Supplementary Information accompanies this paper at <https://doi.org/10.1038/s41467-019-11130-y>.

Competing interests: The authors declare no competing interests.

Reprints and permission information is available online at <http://npg.nature.com/reprintsandpermissions/>

Peer review information: *Nature Communications* thanks Francisco Garcia-Vidal, Xiaojun Wu, and the other anonymous reviewer(s) for their contribution to the peer review of this work.

Publisher's note: Springer Nature remains neutral with regard to jurisdictional claims in published maps and institutional affiliations.



Open Access This article is licensed under a Creative Commons Attribution 4.0 International License, which permits use, sharing, adaptation, distribution and reproduction in any medium or format, as long as you give appropriate credit to the original author(s) and the source, provide a link to the Creative Commons license, and indicate if changes were made. The images or other third party material in this article are included in the article's Creative Commons license, unless indicated otherwise in a credit line to the material. If material is not included in the article's Creative Commons license and your intended use is not permitted by statutory regulation or exceeds the permitted use, you will need to obtain permission directly from the copyright holder. To view a copy of this license, visit <http://creativecommons.org/licenses/by/4.0/>.

© The Author(s) 2019